Layer-by-Layer Deposition of 2D CdSe/CdS Nanoplatelets and Polymers for Photoluminescent Composite Materials

Fuzhao Li[†], Lars F. Klepzig[†], Nils Keppler, Peter Behrens, Nadja C. Bigall, Henning Menzel[*], Jannika Lauth[*]

Abstract

Two-dimensional (2D) semiconductor nanoplatelets (NPLs) are strongly photoluminescent materials with interesting properties for optoelectronics. Especially their narrow photoluminescence paired with a high quantum yield are promising for light emission applications with high color purity. However, retaining these features in solid-state thin films together with an efficient encapsulation of the NPLs is a challenge, especially when trying to achieve high quality films with defined optical density and low surface roughness. Here we show photoluminescent polymer-encapsulated inorganic-organic nanocomposite coatings of 2D CdSe/CdS NPLs in poly(diallyldimethylammonium chloride) (PDDA) and poly(ethylenimine) (PEI), which are prepared by sequential layer-by-layer (LbL) deposition. The electrostatic interaction between the positively charged polyelectrolytes and aqueous phase transferred NPLs with negatively charged surface ligands is used as driving force to achieve self-assembled nanocomposite coatings with well-controlled layer thickness and surface roughness. Increasing the repulsive forces between the

NPLs by increasing the pH value of the dispersion leads to the formation of nanocomposites with all NPLs arranging flat on the substrate, while the surface roughness of the 165 nm (50 bilayers) thick coating decreases to R_a = 14 nm. The photoluminescence properties of the nanocomposites are determined by the atomic layer thickness of the NPLs and the 11-mercaptoundecanoic acid ligand used for their phase transfer. Both, the FWHM (20.5 nm) as well as the position (548 nm) of the nanocomposite photoluminescence are retained in comparison to the colloidal CdSe/CdS NPLs in aqueous dispersion, while the measured photoluminescence quantum yield of 5 % is competitive to state-of-the-art nanomaterial coatings. Our approach yields stable polymer-encapsulated CdSe/CdS NPLs in smooth coatings with controllable film thickness, rendering the LbL deposition technique a powerful tool for the fabrication of solid-state photoluminescent nanocomposites.

Introduction

Two-dimensional (2D) semiconductor nanoplatelets (NPL) are attracting broad scientific interest due to their promising optoelectronic properties, including their anisotropic light emission and a small Stokes shift.[1–4] 2D NPLs are strongly quantum-confined in their thickness dimension, which leads to strong excitonic effects and narrow absorption in the structures as well as efficient photoluminescence (PL) allowing for their use in light emitting applications or lasing.[1–8] Cadmium chalcogenide NPLs, especially CdSe, exhibit high photoluminescence quantum yield (PLQY) and tunable emission in the visible range. By growing a CdS crown in the lateral NPL dimension, the PLQY and stability of CdSe NPLs is significantly enhanced without a red-shift of the NPL PL.[9] Tessier *et al*. showed the successful synthesis of 2D CdSe/CdS core-crown NPLs and increased the PLQY of pristine CdSe NPLs from <10 % to 60 % for core-crown structures. An adapted

procedure for 2D CdSe/CdS core-crown NPLs with varying lateral size, thickness and shape of the crown yielded PLQY values of up to 90 % as has been reported by Schlosser *et al*.[2,5] Since the growth of the crown lacks influence on the thickness of the NPLs, the spectral position of the excitonic CdSe absorption as well as the narrow FWHM of the PL is retained.

The combination of 2D semiconductor NPLs with polymers for the formation of organic-inorganic nanocomposites is a promising approach to obtain functional materials that are easy to handle, while stabilizing the 2D NPLs in an inert matrix.[10] For example, the incorporation of NPLs into conductive polymers enables charge carrier separation, albeit at the cost of PL quenching due to NPL-polymer interactions.[11,12] Retaining the PL properties of the NPLs thus requires a minimum detrimental NPL-polymer interaction and avoiding NPL agglomeration.[13] A highly promising approach to achieve ordered polymer-NPL nanocomposite multilayer films is the layer-by-layer (LbL) dip-coating technique. Here, a sequential and alternating deposition of polyelectrolytes (PEL) and NPLs that are charged oppositely is applied.[14–19] The electrostatic attraction between the charges of the polymers and the NPLs leads to a self-assembly process of the nanocomposites with a controllable layer number on a variety of substrates.[17,20] The choice of suitable PELs that lack electronic interaction with the NPLs is crucial and leads to the NPLs dominating the optical properties of the nanocomposites. However, the PEL species can have significant influence the film structures. Commonly used PELs are divided into two types, strong PELs, such as poly(diallyldimethylammonium chloride) (PDDA), and weak PELs like poly(allylamine) (PAAm) and poly(ethyleneimine) (PEI).[13,18,21] A strong PEL will remain highly dissociated and release counterions in solution over a wide pH range. The charged groups along the polymer chain result in repulsive forces and a stiffening of the polymer chain. [18,21] On the contrary, the dissociation degree of a weak PEL is much more pH-dependent.[18,21,22] During the film formation process, an

adsorbed layer of a weak PEL is able to alter its chain conformation by partially wrapping around incorporated nanomaterials, while no such wrapping phenomenon is observed with strong and stiffer polymer chains like PDDA.[21]

Due to its high potential for the formation of controlled multilayer films with incorporated nanocrystals (NC), combined with a controllable NC concentration, ease of processing, and moderate production costs, the LbL deposition technique has proven to be an efficient method for the fabrication of NC/PEL composite materials.[23–26] The processing of semiconductor NCs using LbL assembly has been studied extensively and functional optical multilayer films have been obtained.[25–27] However, our innovative approach by implementing 2D NPLs with narrow PL FWHM and high PLQY has the potential to significantly improve the optical performance of multilayers, and making the resulting coatings competitive for optical applications.[1,2,28]

Here, we present a facile method to coat substrates with multilayers of CdSe/CdS core-crown NPLs and PELs by LbL deposition to obtain photoluminescent NPL-polymer nanocomposite thin films. We can tailor the structure and the surface roughness of the obtained films by adjusting the degree of ionization using strong and weak PELs and by varying the pH value. The optical properties of the obtained nanocomposite films include an almost similar PL position as for the NPLs in aqueous dispersion and retain the narrow PL FWHM of the aqueous colloidal solution with a competitive PLQY of 5 %.

Results and Discussion

CdSe/CdS core-crown NPLs with a thickness of 4 monolayers (ML) were synthesized according to literature.[5] The NPLs exhibit narrow absorption and PL centered at 515 nm. The growth of a

CdS crown improved the PLQY of the materials drastically from 20 % to 70 % by preventing nonradiative recombination due to trap states along NPL edges.[9,29] CdSe/CdS NPLs were transferred to aqueous dispersion by using a ligand exchange from oleic acid to bifunctional hydrophilic molecules. The ligand with the best ability to retain the PLQY of the NPLs is 11-mercaptoundecanoic acid (MUA).[30] The thiol group exhibits high affinity to the Cd-terminated NPL surface and the carboxylate group provides the hydrophilicity to assure the water-solubility of the NPLs (Figure 1). In alkaline solution, the carboxylate groups are deprotonated, creating negative charges near the NPLs. This generates repulsive forces between individual NPLs and prevents agglomeration, thus ensuring the colloidal stability of the NPLs in aqueous dispersion.[13] Additionally, negatively charged MUA ligands on the NPLs provide the possibility for their arrangement into bilayers with positively charged PELs by LbL deposition. We used PDDA and PEI (see Figure 1a) as strong and weak PELs. PDDA and PEI lack effects on the optical properties of the NPLs in LbL assemblies, in contrast to poly(allylamine) (PAAm), which was discarded for further characterization (see Figure S1). Both, PDDA and PEI possess amino groups along the polymer chains with PDDA carrying quaternary ammonium groups that are positively charged independently of the pH. Because of the repulsive forces, the polymer chain is stretched to some extent. Furthermore, the ring structure in the polymer chain (see Figure 1a) decreases the chain flexibility.[31] On the other hand, PEI possesses secondary amino groups mainly. However, since it is branched, additional tertiary and primary amino groups are present at the branching points and as end groups, respectively (see idealized structure in Figure 1a). All these amino groups can be protonated in aqueous solution depending on the pH, thus leading to PEI being mildly charged at high pH values and strongly charged at low pH values.[32] Both, the quaternary ammonium groups of the PDDA as well as the protonated amino groups provide positive charges of the PEI for the

adsorption of negatively charged NPLs, yet they differ significantly in terms of chain flexibility and charge density.[14,15,21] The pK_a values of primary and secondary amino groups on weak PELs are sensitive to their local ionic environment and become lower in the solid state than in aqueous solution.[33,34] This results in less charged and more flexible polymer chains of weak PELs like PEI, which can alter their conformation flexibly during a deposition process. On the contrary, PDDA as strong PEL has numerous quaternary ammonium cations, which remain positively charged irrespective of the pH value over a wide range.[35] Correspondingly, PDDA exhibits a less flexible polymer chain; together with the higher number of repulsive charges this results in a more extended conformation.

Figure 1c shows photographs of a glass substrate coated with NPL/PDDA nanocomposites under ambient light and UV irradiation respectively. The covered substrates exhibit a light-yellow color and green PL at 548 nm due to the incorporated CdSe/CdS NPLs (a scheme of the LbL process yielding the coatings is shown in Figure 1d). Silicon wafers and quartz glass coverslips were used as substrates for the deposition. Both of them are negatively charged after rinsing, which can be attributed to the reaction of their native oxide layers with water. The LbL process is started by dipping the respective substrate into the polycation solution, upon which a first PEL layer is formed. The adsorption of the polycation layer leads to a reversal and overcompensation of the original surface charge, which is important for the adsorption of the following NPL layer. The carboxylate groups on the MUA ligands of NPLs are negatively charged and enable the colloidal stability of the NPLs in aqueous solution. For an alternating layer formation with the polycations, the substrates are immersed in a NPL dispersion. Each adsorption step leads to a reversed surface charge, which ensures the continuation of the adsorption process with the sum of one cationic and one anionic layer called a bilayer. The ion amount of PEL and NPLs adsorbed for each single layer

is self-limiting due to the charges, allowing for a precise control over the thickness of the coating. The dipping solutions were prepared as described in the Experimental Section. Each dipping cycle consisted of 10 min of dipping into the PEL solution or the NPL dispersion, respectively, followed by a washing step with deionized water to remove loosely bound molecules and drying under a gentle nitrogen flow.

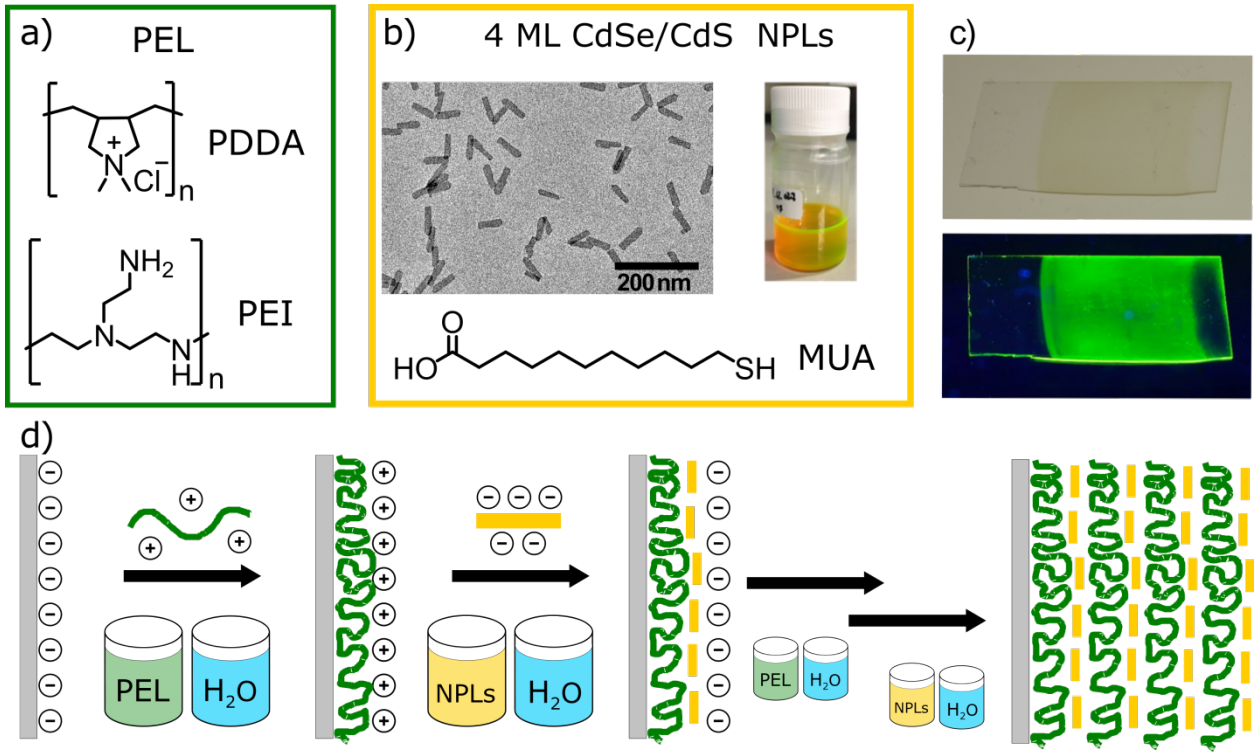

Figure 1: Schematic illustration of a LbL dip-coating process with PDDA, PEI and CdSe/CdS NPLs. a) Idealized molecular structure of PDDA and PEI. b) Transmission electron microscopy (TEM) image of 4 ML CdSe/CdS NPLs and a colloidal dispersion of the NPLs as well as the capping ligand MUA. c) Images of the PDDA/NPL composite LbL film under ambient light (top) and under illumination with UV light (bottom). d) Scheme of the LbL dip-coating process. A substrate (Si or glass, grey) is first dipped into the PEL solution (PDDA or PEI, green), followed by a washing step in deionized water, then dipped in a NPL dispersion (yellow), followed by

another washing step. Due to the opposite charges of the PEL and the MUA capping ligands of the NPLs, a single layer with limited thickness is coated each time. This process can be repeated to achieve the desired film thickness.

The LbL process allows for the subsequent addition of a desired number of PEL/NPL bilayers and thus a precise control on the nanocomposite thickness. The rectangular inorganic CdSe/CdS NPLs (see Fig. 1b and 2a) have a thickness of 4 ML, which is assigned to a zincblende structure with four layers of selenium and five layers of cadmium.[36,37] The NPLs are surface-capped by cadmium, explaining the high affinity to the thiol group of the MUA ligands *via* a Lewis acid base interaction. At the same time, the NPLs' surface is passivated and the net positive charge resulting from the cadmium surplus of the structure is compensated by the MUA ligands. Figure 2a includes a scheme of the high binding strength of the cadmium on the NPL surface to the MUA thiol groups leading to a good surface coverage. This is underpinned by negatively charged MUA carboxylate groups interacting with the positively charged PELs for the formation of a bilayer. While LbL assemblies including weak PELs usually exhibit a complex, nonlinear growth mechanism, we find that using PDDA as strong PEL yields a nearly linear relation between the thickness and the number of layers as shown in Figure 2c.[38,39] Each bilayer adds 7.8 nm ± 0.4 nm to the film thickness according to the linear fit, which is in good agreement with literature values.[40]

With an average CdSe/CdS NPL size of 13.2 x 53.4 nm^2 and a thickness of 1.2 nm (see Figure S2 for a size histogram), we infer that NPLs will be incorporated lying flat-on into the multilayer nanocomposite coating. This ordered deposition of the NPLs in their polymer matrix could be beneficial for using their anisotropic optical properties including a directed PL perpendicular to their plane in future applications.[41]

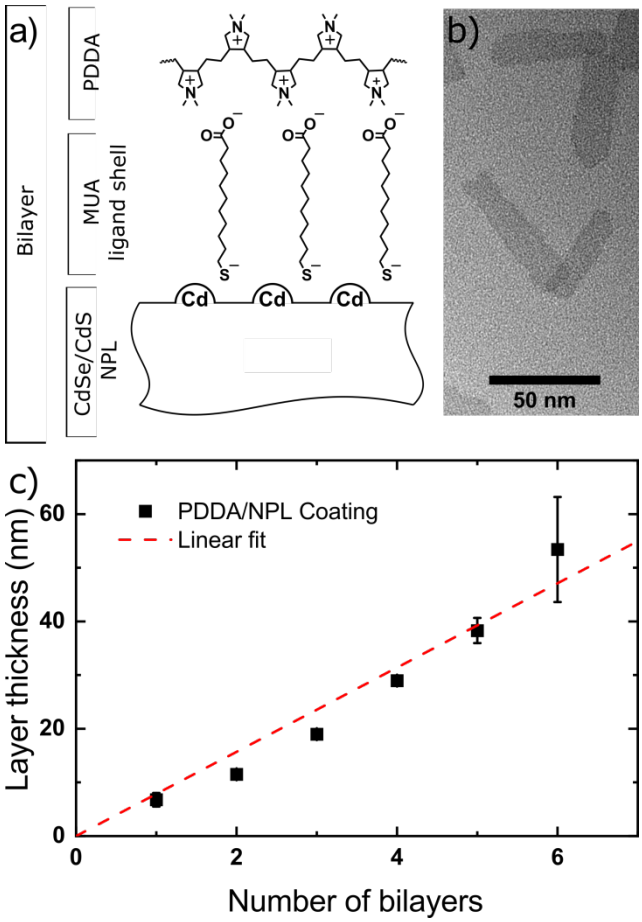

Figure 2: a) Schematic of a PDDA/NPL bilayer and corresponding interplay of the opposite charges within the bilayer. The inorganic part of the CdSe/CdS NPLs is cadmium-terminated, leading to a strong interaction with the thiol groups in MUA ligands, which in turn carry carboxylate groups that ensure adsorption of positively charged PDDA. b) TEM image of rectangular 4 ML CdSe/CdS NPLs with representative NPLs with a lateral dimension of 13.2 x 53.4 nm^2 and a thickness of 1.2 nm. c) Nanocomposite film thickness determined by ellipsometry measurements *vs*. the number of bilayers applied to the substrate. When using PDDA as strong PEL, a linear thickness growth of the assembled films with the increase of deposition cycles is observed.

The negative surface charge of the NPLs was quantified by zeta-potential measurements and adjusted by varying their pH value (see Figure S3). The zeta-potential of the NPL dispersion decreased with increasing pH values, exhibiting negative values over the whole pH-range of 4 – 13 (values ≤ -50 meV for pH ≥ 6) due to the negative charges carried by the carboxylate groups of the MUA ligands. Strong PELs such as PDDA exhibit numerous positive charges along the polymer chain with small pH dependence, while the number of positive charges in weak PELs such as PEI strongly depends on the pH. This influences the coiling of the PEI and thus the thickness and the quality of the resulting nanocomposite films as discussed below.[43,44] Consequently, we kept the PEL solution at a set pH value upon dissolution in deionized water (pH 6.1 for PDDA, pH 10.4 for PEI) and only adjusted the pH value of the NPL dispersion (pH values of 6 and 10 for PDDA and PEI respectively). Lower pH values than 6 led to a destabilization of the NPLs leading to their agglomeration, while higher pH values may lead to a quenching of the NPL PL by the high amount of hydroxide in solution.[42]

The surface morphology of the bilayers is analyzed by atomic force microscopy (AFM, see Figure 3). At pH values of 6, the zeta-potential of the NPLs is low (ζ_{pH6} = -48 mV), while both PDDA and PEI are highly charged. This leads to strong electrostatic attractions with only small inter-NPL repulsion, resulting in bilayers with high NPL concentrations (see Figure 3a, c). Due to its highly charged backbone, PDDA shows an extended conformation of the polymer chains.[21,35,43] This leads to the formation of densely packed PDDA/NPL layers with only little overlap between single NPLs (see Figure 3c). On the contrary, the less charged PEI with a branched polymer chain adjusts its conformation to best "accommodate" the NPLs and wraps around them (see Figure 3a).[21] At a pH of 10, higher inter-NPL repulsive are present due to a more negative zeta potential of the NPLs (ζ_{pH10} = -80 mV). This is observed independently of the use of PDDA or PEI

as PELs, respectively (see Figure 3b, d). As stated before, there is a minor influence of the pH on the zeta-potential of PDDA as strong PEL (ζ_{pH6} = 44.9 mV, ζ_{pH10} = 36.6 mV). At a pH of 10, PDDA still carries enough positive charges to provide attractive forces for NPLs. This results in a well-separated adsorption of NPLs lying parallel to the surface of substrate (see Figure 3d). On the other hand, the zeta-potential of the weak PEL PEI decreases significantly from ζ_{pH6} = 51 mV to ζ_{pH10} = 17.8 mV as the pH is increased from 6 to 10. Due to the lack of sufficient positive charges, adsorption of NPLs to the PELs should be dominated by short-range forces such as hydrogen bonding, hydrophobic forces, and VAN DER WAALS interactions.[21,33,34] However, we find that due to the high repulsive forces among NPLs, the density of NPLs was low and films are nicely packed. We have considered local changes of the pH near the substrate surface due to the different pH values of the NPL and PEL solutions as well. However, since PDDA only shows little pH dependence of its zeta potential, any increase of the pH due to the deprotonated MUA ligands on the NPLs does not exert a significant change on the charge density of PDDA or its rigid backbone structure. On the other hand, combining the PEI solution (pH 10.4) with NPLs dispersed at pH 6 leads to increased absolute values of the zeta potentials of both components, as the carboxyl group of the MUA can protonate the amino groups of PEI. This will increase the attractive interaction, while also increasing the inter-NPL repulsion and thus reducing, albeit not preventing, the formation of unordered NPL/polymer clusters as shown in Figure 3a. Despite this unfavorable interaction, highly ordered films using PEI can be achieved by increasing the pH value of the NPL dispersion, which is also the crucial parameter to adjust the NPL concentration in PDDA films.

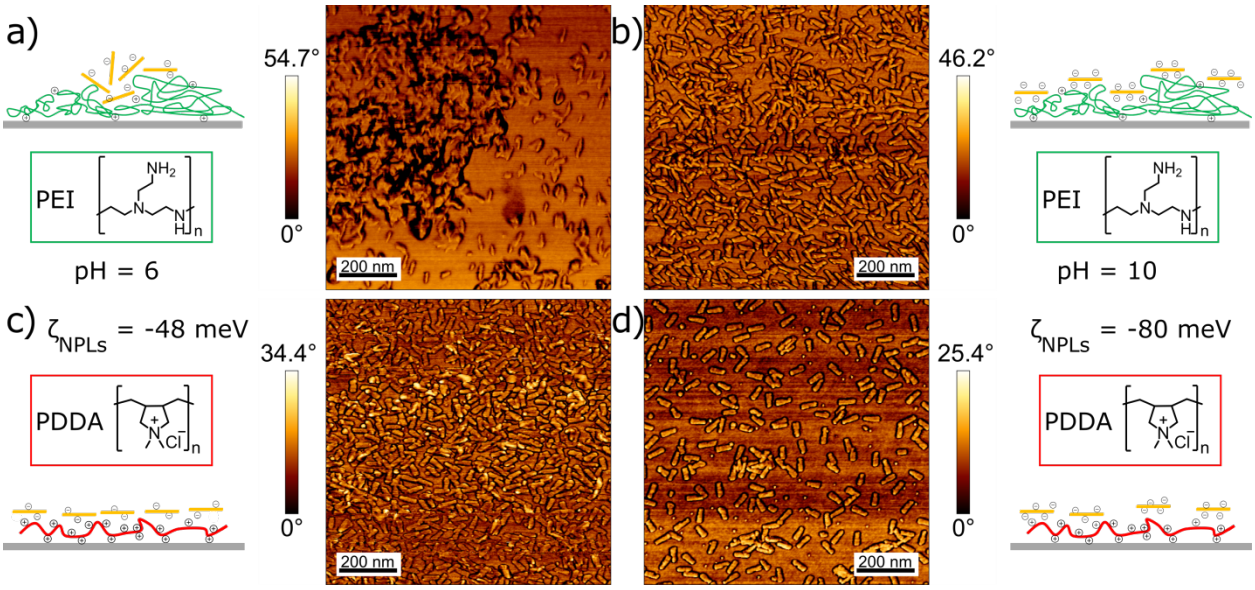

Figure 3. PEL and NPL pH value influence on the LbL coating process with AFM phase images of a single bilayer taken in an area of 1 x 1 μm^2 and schemes of the formed surface coating. The combination of a) PEI with NPLs at pH 6, b) PEI with NPLs at pH 10, c) PDDA with NPLs at pH 6, and d) PDDA with NPLs at pH 10. By controlling the pH value of the NPL dispersion, we can control the number of charges per NPL as shown by the zeta potential values and discussed in the text. Corresponding AFM height images of samples can be found in Figure S4.

Besides the electrostatic interactions between the charged PELs and the oppositely charged NPLs entropic contributions have to be considered as well.[18,44,45] PELs show counterion condensation, that is, the counterions are partially not released into the solution but are close to the ionic groups at the polymer chain to compensate the charge. By this the charge density along the polymer chain is reduced below a critical value which is given by MANNING's theory or its refinements.[46,47] During the LbL assembly process, the ionizable units of a PEL can release counterions and be neutralized by the oppositely charged NPLs.[48] The release of the counterions from the PEL as well as from the NPLs results in a entropic gain, which represents a strong driving force for the formation of the LbL films.

The interpretation of AFM measurements on individual bilayers of the nanocomposites in Figure 3 can be extended to profilometry studies of the PEL/NPL nanocomposite coatings with a thickness of 50 bilayers (see Figure 4, Table 1 and Figure S5 for height histogram). The analysis of the surface roughness shown in Figure 4a underpins that higher pH values used for the NPL dispersion lead to the formation of smooth surfaces with high optical quality, with PDDA and at pH 10 yielding the lowest surface roughness (arithmetic average roughness R_a = 14 nm). A comparable value of R_a = 18 nm is achieved by using PEI at pH 10 supporting the results of the AFM measurements that all NPLs are lying flat-on and that little overlap of separate NPLs is observed. Decreasing the pH value of the NPL dispersion to pH 6 increases the surface roughness, as the repulsive forces between the NPLs are reduced and the NPL concentration in one bilayer increases (R_a= 42 nm and R_a = 59 nm for PDDA and PEI with NPLs at pH 6, respectively). The same trend gets apparent when calculating the root mean squared roughness R_q (see Table 1). The R_q accentuates larger deviations from the mean value, leading to higher values when the surface roughness possesses a high amplitude. Here, in good agreement with the R_a values, we find nanocomposite coatings deposited with NPL dispersions at pH 10 yield low R_q values of R_q = 22 nm and R_q = 32 nm with PDDA and PEI respectively.

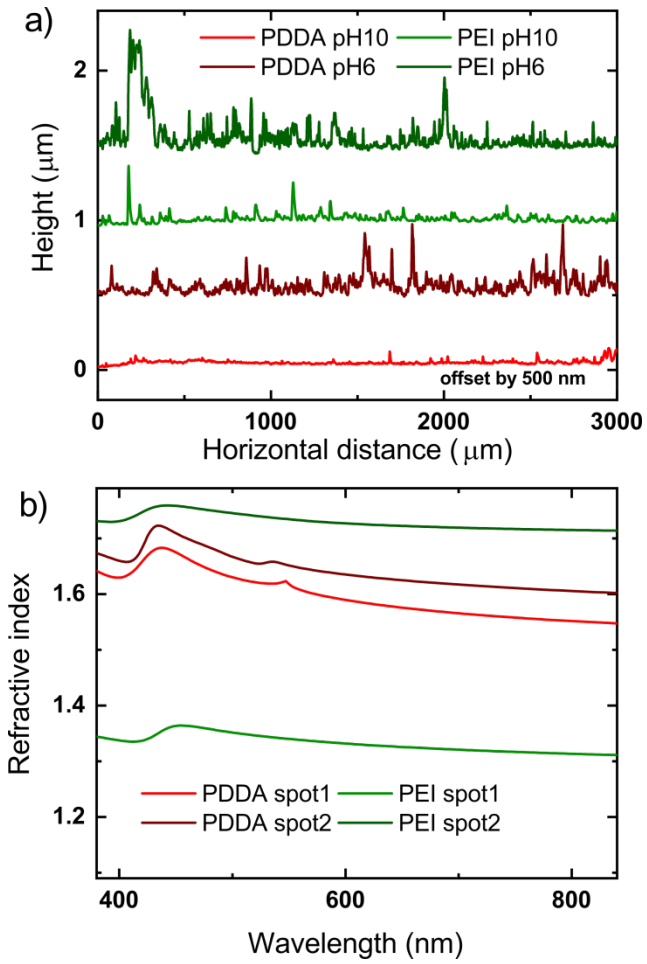

Figure 4: Surface roughness of the PEL/NPL nanocomposite layers. a) Profilometry measurements of nanocomposites with 50 bilayers using PDDA and PEI and a pH value of the NPL dispersion of 6 and 10, respectively. The lowest surface roughness is obtained in nanocomposites with PDDA as PEL and pH 10 for the NPL dispersion. b) Refractive index measurements of 50 bilayers of PDDA/NPL and PEI/NPL layers on Si, deposited at a pH value of 10. Nanocomposites with PEI generally show higher deviations between measurement spots.

Table 1: Height and surface roughness of LbL nanocomposite films with a thickness of 50 bilayers as determined by profilometry measurements. Height measurements were performed on each sample at ten different lines with a scan length of at least 2 mm, while the surface roughness was determined with three measurements over at least 3 mm.

	PDDA pH10	PDDA pH6	PEI pH10	PEI pH6
Height (nm)	165 ± 10	170 ± 20	150 ± 40	180 ± 50
R_a (nm)	14	42	18	59
R_q (nm)	22	65	32	91

The refractive index of PEL/NPL nanocomposite coatings was determined using ellipsometry. The data are fitted with a Tauc-Lorentz plot and are in good agreement with the measured data (mean square error (MSE) < 6, see Figure S6).[49] When using the weak PEI as PEL for nanocomposite deposition, strong refractive index differences between different spots on the film are found and indicate inhomogeneities (refractive indices between 1.75 and 1.30 are obtained, see Figure 4b). Nanocomposites with PDDA as PEL on the other hand show only minor deviations in the refractive index between different spots of the film (see Figure 4b). This is in good agreement with AFM and profilometry measurements as discussed above, showing that highly homogeneous films are achieved by the LbL method with strong PELs such as PDDA.

The film thickness of the nanocomposites as is determined by profilometry is listed in Table 1 (exemplary measurement and evaluation, see Figure S7). A nanocomposite film thickness of 160 to 180 nm is found, with the magnitude of the deviation between different measurement spots following the same trends as discussed above (lowest for PDDA pH 10, highest for PEI pH 6). It has to be noted that the height is lower than expected (390 nm if each bilayer has a thickness of 7.8 nm) from the linear relation established in Figure 2c), indicating that the layer growth slows down after reaching a large number of bilayers.

For characterizing the influence of the PEL/NPL bilayer formation on the optical properties of the nanocomposites, we measured the absorption and PL of the samples as well as their PL lifetimes

(LT) by time-correlated single photon counting (TCSPC). To exclude interactions between the substrate and the PEL/NPL nanocomposites leading to a quenching of the PL, a spacer coating of 10 bilayers of negatively charged poly(styrenesulfonic acid) (PSS) and PDDA were deposited before forming the LbL films with the NPLs for the PLQY measurements. Figure 5a shows that the absorbance and PL of the CdSe/CdS NPLs shift bathochromically (from 515 nm to 543 nm, $\Delta\lambda_{PL} = 28$ nm, 124 meV) during the phase transfer from organic to aqueous dispersion. The thiol layer of the MUA ligand acts as a quasi-sulfide layer, effectively increasing the thickness of the NPLs.[30,50,51] Transferring the aqueous NPL dispersion to the PEL/NPL nanocomposite, however, only induces a small bathochromic shift (543 nm to 548 nm, $\Delta\lambda_{PL} = 5$ nm, 21 meV), assumedly caused by changes in the vicinity of single NPLs such as different dielectric constants of the polymer matrix compared to water.[52]

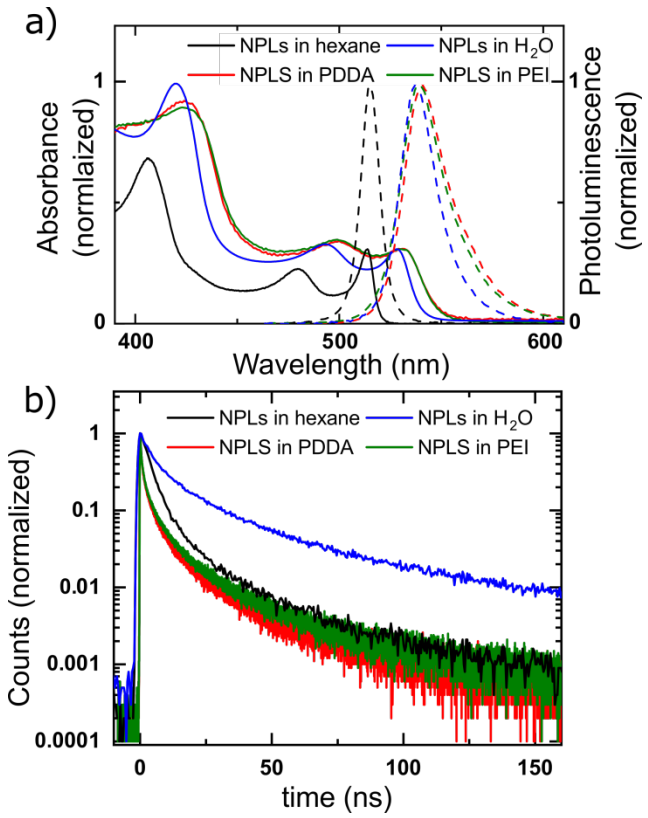

Figure 5: Absorption and PL (dashed) of CdSe/CdS NPLs dispersed in hexane, after their ligand exchange with MUA in aqueous dispersion and after the deposition as nanocomposites with PDDA and PEI by LbL. Absorption and PL spectra are shown for 50 bilayers deposited with the NPL dispersion held at pH 10. a) A bathochromic shift (515 nm to 543 nm, $\Delta\lambda_{PL} = 28$ nm, 124 meV) of the absorption and PL of the CdSe/CdS NPLs is apparent after the phase transfer, while the change upon formation of the nanocomposites is only minor (543 nm to 548 nm, $\Delta\lambda_{PL} = 5$ nm, 21 meV). The absorbance is normalized to the first excitonic absorption maximum of the NPLs, while the PL is normalized to the maximum value. b) The PL LT values of CdSe/CdS NPLs increase after the phase transfer due to the MUA ligands forming a quasi-S shell that leads to an increased delocalization of electrons followed by a strong decrease of the PL LTs in LbL films. Shorter PL LTs in the nanocomposites most likely originate from the few film regions where NPLs overlap or are packed very closely and exhibit interaction with each other despite the PEL passivation. These close interactions are not present in the dispersions.

The negligible change in absorption and PL after the LbL process underpins the successful encapsulation of the NPLs into the polymer matrix without detrimental charge carrier or energy transfer interactions in the nanocomposites. The PELs investigated do not show any absorption or PL in the NPL wavelength range where theses phenomena are observed for the NPLs (see Figure S8), emphasizing that the optical properties of the LbL nanocomposite coatings are strongly dominated by the NPLs. Additionally, the optical properties of the nanocomposites by using PDDA and PEI as PELs (see Figure 4), or when adjusting the pH value (see Figure S9) remain identical, meaning that these parameters do not influence the optical properties.

The PL FWHM increases from 7.4 nm to 15.7 nm due to the thiol groups necessary for the phase transfer and an associated thickness increase of the NPLs. The PL spectra of the PEL/NPL

nanocomposites exhibit a FWHM of 20.5 nm and 22.0 nm for PDDA and PEI used as PEL, respectively, which is only slightly broader than the FWHM of NPLs in aqueous dispersion. With a FWHM of 20 nm, the PEL/NPL nanocomposites shown here are able to compete with state-of-the-art NCs in organic dispersion (typically $\geqslant$ 20 nm), rendering the materials competitive for high purity light emission.[53–56]

The PL properties of the NPLs in the nanocomposite films depend on the distance between single NPLs and is predominantly governed by the length and functionality of the ligand shell covering them. Since the substrate for the LbL deposition of the PEL/NPL nanocomposite is charged positively by the first PEL layer, negatively charged MUA ligands on the NPL surface interact with them forming a stable bilayer. This process is even more efficient the higher the ligand density is, ensuring that only NPLs with an intact ligand shell are incorporated into the nanocomposite. This also ensures a low density of surface traps by missing ligands.

Figure 5b shows the PL LT of the CdSe/CdS NPLs in organic and aqueous dispersion after the ligand exchange and after the LbL deposition. We find no influence of the PEL or the pH on the resulting optical properties (see Figure S9). An increase of the PL LT from 4.4 ns ± 0.1 ns to 7.9 ns ± 0.1 ns after the phase transfer of the NPLs is caused by their thickness increase due to the quasi-S layer of the MUA ligands, which leads to a delocalization of electrons into the ligand shell and decreases the electron-hole overlap (holes are more localized in the CdSe core).[30,51] The PL LT of NPLs in hexane and aqueous dispersion are fitted biexponentially with two time constants $\tau_{1hex} = 3.6\ \text{ns} \pm 0.4\ \text{ns}$, $\tau_{2hex} = 19.2\ \text{ns} \pm 0.5\ \text{ns}$, $\tau_{1aq} = 4.1\ \text{ns} \pm 0.3\ \text{ns}$, and $\tau_{2aq} = 23.5\ \text{ns} \pm 0.7\ \text{ns}$ respectively. The contribution of τ_{2aq} increases due to the delocalization of the electrons into the ligand shell. After the LbL deposition, we find a shorter PL LT $\tau_{average}$ of

0.9 ns ± 0.1 ns in both, the PDDA/NPL and PEI/NPL nanocomposites with an additional fast recombination process, which is fitted with the time constant $\tau_{short-PDDA} = 0.5$ ns ± 0.1 ns and $\tau_{short-PEI} = 0.5$ ns ± 0.1 ns. Interactions between closely packed individual CdSe/CdS NPLs or between NPLs and the amino groups of the polymer are possible reasons for faster charge carrier recombination, as suggested by literature.[13,57] This suggests a non-optimal passivation by the MUA ligands, either because of incomplete coverage or insufficient distance between the NPLs.

Table 2: PL and PLQY of CdSe/CdS NPLs in hexane, after phase transfer to aqueous dispersion and as PEL/NPL LbL nanocomposite coatings with additional PSS/PDDA spacer coating on the substrate.

	Position PL	**FWHM PL**	**PLQY**	**$\tau_{average}$ (ns)**	**τ_{short} (ns)**	**τ_1 (ns)**	**τ_2 (ns)**
CdSe/CdS NPLs in hexane (*hex*)	515 nm	7.4 nm	70 %	4.4	-	3.6	19.2
CdSe/CdS NPLs in H_2O (*aq*)	543 nm	15.7 nm	35 %	7.9	-	4.1	23.5
PDDA/CdSe/CdS NPL nanocomposite	548 nm	20.5 nm	4.7 %	0.9	0.5	4.0	22.6
PEI/CdSe/CdS NPL nanocomposite	548 nm	22.0 nm	5.3 %	0.9	0.5	4.0	24.3

The PL properties and PLQY of the pristine and ligand-exchanged NPLs as well as the PEL/NPL nanocomposites are summarized in Table 2. The PLQY of the NPLs decreases by the phase transfer (from 70 % to 35 %), induced by hole traps originating from the MUA thiol ligand.[58,59] The nanocomposite coatings exhibit a PLQY of 4.7 % and 5.3 % for PDDA/NPL and PEI/NPL

films, respectively. This is in line with PLQY values typically reported for solid-state thin films.[13,51,60] While higher PLQY values in solid-state films have been observed using core/shell NCs (PLQY 27 %) with a spin-coated film of PbS/CdS NCs and a PLQY of 24 % with a silica shell around CdTe NCs, the introduction of a shell to the NCs leads to a significant broadening of their PL (e.g. from 35-40 meV to 62-90 meV for CdSe NPLs and CdSe/CdS core-shell NPLs).[28,60,61] Our approach combines retaining narrow PL FWHM values of 20 nm in photoluminescent smooth PEL/NPL nanocomposite coatings with a controllable film thickness and an efficient PLQY of 5 %, while at the same time enabling a stable polymer encapsulation of the colloidal CdSe/CdS NPLs. This provides a procedure to shape photoluminescent NPLs into a solid-state form which is typically used in optical devices.

Conclusion

We have investigated a LbL deposition process for the fabrication of polymer matrix-encapsulated photoluminescent CdSe/CdS NPLs nanocomposites as optically active film coatings. Negatively charged ligands on the phase transferred NPLs' surfaces allow for the interaction with the positively charged PELs and the formation of bilayers. The choice of the polymer determines the homogeneity and surface roughness of the nanocomposite coatings, with PEI causing higher thickness deviations (R_a = 59 nm) due to polymer coiling around the NPLs. Adjusting the pH of the aqueous CdSe/CdS NPL dispersion to pH 10 resulted in the formation of flat-on oriented NPLs in the LbL coatings independent of the choice of polymer and yielded smooth layers with R_a values of 14 nm and 18 nm using PDDA and PEI as PEL, respectively. Additionally, the pH value can be used to adjust the NPL concentration in the PDDA films. A PLQY of ~5 % is obtained for PEL/NPL nanocomposites, which is competitive to state-of-the-art colloidal nanomaterial coatings

and allows for the formation of photoluminescent smooth nanocomposite thin films by retaining the NPL optoelectronic properties.

Experimental Section

Chemicals. Sodium myristate (≥ 99 %), acetone (99.5 %), methanol (MeOH, ≥ 99.8 %), 1-octadecene (ODE, 90 %), sulfur (99.98 %), 11-mercaptoundecanoic acid (MUA, 95 %), n-hexane (≥ 99 %), ethanol (EtOH, ≥ 99.8 %), poly(allylamine) (PAAm, 10 wt% in H_2O), poly(ethylenimine) (branched, PEI, 99 %), poly(diallyldimethylammonium chloride) (PDDA, 20 wt% in H_2O), and potassium hydroxide (KOH, 85 %) were supplied from Sigma Aldrich. Cadmium nitrate tetrahydrate (99.999 %), selenium (99.999 %, 200 mesh), poly(styrenesulfonic acid) (PSS, 30 wt% in H_2O) and oleic acid (HOA, 90 %) were supplied by Alfa Aesar. Cadmium acetate dihydrate ($Cd(Ac)_2$, 98 %), hydrochloric acid (HCl, 37 %), and tri-*n*-octylphosphine (TOP, 97 %) were purchased from ABCR. Chloroform (99.96 %) was purchased from Fischer. All chemicals except for ODE were used as received without further purification. ODE used for the preparation of the chalcogenide precursor solutions was purified by degassing it at 120 °C under oil pump vacuum ($p \leq 1 \times 10^{-3}$ mbar) for at least 6 h. Afterwards, the purified ODE was stored in an air-free glove box.

Synthesis of CdSe core nanoplatelets (NPLs). CdSe NPLs with a thickness of 4 monolayers (ML) were synthesized according to Ithurria *et al*.[36] Cadmium myristate ($Cd(myr)_2$) was prepared according to Tessier *et al*.[2] Briefly, in a three-neck flask, 1360 mg (2.4 mmol) $Cd(myr)_2$ and 96 mg (1.2 mmol) Se were dispersed in 120 mL ODE and degassed under vacuum for 60 min at 70 °C. Subsequently, the mixture was heated to 240 °C under Ar atmosphere. At 205 °C, 240 mg (1.0 mmol) $Cd(Ac)_2$ were added. After 12 min, the synthesis was stopped by the addition of 8 mL HOA and allowed to reach room temperature. 40 mL of a 2:1 mixture of EtOH and hexane were added, and the dispersion centrifuged at 4000 rcf for 10 min. The colorless supernatant was discarded and the precipitated CdSe NPLs redispersed in 10 mL of hexane.

Synthesis of CdSe/CdS core-crown NPLs. The growth of the CdS crown around the CdSe core NPLs was performed according to Schlosser *et al*.[5] Briefly, 1.165 mL of core CdSe NPLs in hexane (c_{Cd} = 40.0 mM, β_{CdSe} = 7.64 mg L^{-1} as measured by AAS) were combined with 180 μL (0.6 mmol) HOA, 96 mg (0.4 mmol) $Cd(Ac)_2$ and 8 mL ODE in a three-neck flask. The hexane was removed carefully under oil pump vacuum *via* the Schlenk line at room temperature and the mixture was further degassed under vacuum for 1 h at 60 °C. Under an Ar atmosphere, the solution was then heated to 240 °C. Starting at 215 °C, 6 mL of a 0.05 M solution of S in ODE was injected at a rate of 18 mL h^{-1}. After completion of the injection, the solution was kept at 240 °C for additional 10 min before it was rapidly cooled down to room temperature. To precipitate the CdSe/CdS NPLs, 10 mL of a 2:1 mixture of EtOH and hexane were added, followed by a centrifugation at 4000 rcf for 10 min. The core-crown CdSe/CdS NPLs were redispersed in 2 mL hexane.

Phase transfer of CdSe/CdS core crown NPLs to aqueous dispersion. The phase transfer was performed according to Kodanek *et al*.[30] Briefly, 4 mL of a CdSe/CdS NPL dispersion (c_{Cd} = 20.0 mM) were mixed with a solution of 0.070 g (0.3 mmol) MUA and 0.040 g (0.7 mmol) KOH in 5 mL MeOH and shaken overnight. Subsequently, the colorless hexane phase was removed and the now yellow MeOH phase was centrifuged at 4000 rcf for 10 min. The precipitated CdSe/CdS NPLs with MUA ligands were redispersed in 4 mL aqueous KOH (0.1 M).

Substrate preparation. The layer-by-layer (LbL) dipping processes was performed on glass and silicon substrates in order to characterize the optical properties and surface morphology of the inorganic/organic multilayer assemblies, respectively. Both microscope coverslips (LH24.1, Roth) and one-side polished silicon wafers (125 mm, Ultrapark, Entegris) were cut into small rectangles (1 × 2 cm^2) followed by sonication in chloroform, acetone, EtOH and deionized water.[38] After drying the substrates with nitrogen, they were stored in well plates for further experiments.

Preparation of LbL dipping dispersions: CdSe/CdS core-crown NPLs were prepared by diluting the phase transferred colloidal NPL dispersion with Millipore water to a concentration of 0.05 mg mL^{-1} (Cd^{2+} reference). The NPL dispersions were stored in a dark cabinet for further use. The preparation of polyelectrolyte (PEL) solutions were carried out according to Sydow *et al*.[38] Briefly, the PELs were dissolved or diluted in Millipore water to obtain a standard solution with a PEL concentration of 1 mg mL^{-1}. For characterizing the influence of the pH on the formation of LbL multilayers, a 0.1 M HCl solution was used to adjust the pH of NPL dispersions.

LbL dip-coating process: The preparation of multilayer samples was performed through LbL dip coating using a dip robot (DR-3, Riegler & Kirstein) according to Sydow *et al*. and Shavel *et. al*.[38,62] Briefly, silicon- or glass substrates were first dipped into a PEL solution for 10 min, followed by rinsing in deionized water for 1 min and drying with a gentle flow of nitrogen. Subsequently, the samples were dipped in a NPL dispersion for 10 min with rinsing in water for 1 min and finally drying with nitrogen again. A multilayer structure with a certain number of bilayers was formed by repeating this process. The dipping time and number of cycles can be controlled in advance by programming the dip robot.

UV-Vis absorption and photoluminescence (PL) spectroscopy. The samples for UV-vis absorption and PL spectroscopy were prepared by diluting the CdSe/CdS NPL dispersions in quartz cuvettes with a path length of 10 mm with hexane or water, respectively, to achieve an optical density (OD) of < 0.2 at the first excitonic absorption feature or the excitation wavelength, respectively. The deposited LbL samples were characterized by using a solid sample holder. Absorption spectra were acquired on a Cary 5000 spectro-photometer from Agilent Technologies. Steady-state PL emission spectra and lifetime measurements (time-correlated single photon counting, TCSPC) were measured using an Edinburgh FLS 1000 UV-Vis-NIR PL spectrometer.

The steady-state PL was collected by exciting the samples at 450 nm with a xenon lamp and utilizing a PMT detector. The photoluminescence quantum yield (PLQY) was determined by utilizing an integrating sphere, comparing the amount of photons absorbed to those emitted as described in literature.[63] The TCSPC measurements were carried out using a Picosecond Pulsed Diode Laser (EPL) with a wavelength of 445.1 nm and a pulse length of 110 ps by Edinburgh Instruments.

Atomic absorption spectroscopy (AAS). Atomic absorption spectroscopy to determine the Cd ion concentration in CdSe/CdS NPLs was carried out on a Varian AA140 instrument equipped with an air/acetylene (1.5:3.5) flame atomizer. 5 – 15 μL of a NPL dispersion were dissolved in *aqua regia* overnight, before the solution was filled up to 50 mL with Millipore water (R = 18.2 MΩ cm) in 50 mL round-bottom flasks. For a calibration curve, at least 5 standard solutions in the concentration range between 0 and 2.5 ppm were analyzed.

Transmission electron microscopy (TEM). TEM measurements were performed with a FEI Tecnai G2 F20 transmission electron microscope equipped with a field emission gun operating at 200 kV. The CdSe/CdS NPL samples were prepared by drop casting a diluted dispersion of the NPLs onto a carbon coated copper grid (300 mesh) from Quantifoil.

Dynamic light scattering (DLS): The zeta-potential of CdSe/CdS NPL dispersions after their phase transfer was measured using a Zetasizer (Nano ZS, Malvern Instruments). Data evaluation was performed using the software Malvern Zetasizer Version 7.03.

Atomic force microscopy (AFM): The surface morphology of the deposited CdSe/CdS NPL-polymer nanocomposite LbL coatings on silicon substrates was investigated with an atomic force microscope (XE 100, Park Systems). All measurements were carried out in tapping mode with a 1 μm^2 piezoscanner. For imaging analysis, the software JPK Data Processing was used.

Ellipsometry: The film thickness PEL/NPL nanocomposites was measured by a Multiskop (Optrel) in Null ellipsometry-mode. Measurements were carried out in x,y-mode with an angle of incidence of 70° and 60°. The results were evaluated with the ellipsometry software Version 3.2. The determination of the refractive index by ellipsometry measurements was performed using a Sentech SE800 spectroscopic ellipsometer with a spectral range of 370 to 850 nm. The experimental data for Psi (Ψ) and Delta (Δ) were taken at angles of incidence of 60° and 70°. For fitting the data, a Tauc-Lorentz model with 3 oscillators was used. The starting point for the band gaps of the oscillators were chosen with respect to the absorption bands in the UV/Vis spectrum of the NPLs.

Profilometry (Dektak®). The surface roughness of the PEL/NPL nanocomposite films was determined by Profilometry with a Dektak 8 advanced development profiler by Veeco. The samples were prepared by dip-coating 50 bilayers onto a Si wafer. For the surface roughness measurements, at least three measurements over a distance of 3 – 10 mm were taken for each sample. For the thickness measurements, the sample was scratched to expose the substrate and at least ten measurements over a distance of 3 mm were taken perpendicular to the scratch. Both the preparation and the measurement of the samples were performed under air in a normal laboratory fume hood, without the exclusion of dust particles which can detrimentally contribute to the surface roughness.

AUTHOR INFORMATION

Corresponding Authors

Henning Menzel - Cluster of Excellence PhoenixD (Photonics, Optics, and Engineering – Innovation Across Disciplines), Hannover, Germany; Institute for Technical Chemistry, Technische Universität Braunschweig, Hagenring 30, 38106 Braunschweig, Germany

h.menzel@tu-braunschweig.de

Jannika Lauth - Cluster of Excellence PhoenixD (Photonics, Optics, and Engineering – Innovation Across Disciplines), Hannover, Germany; Institute of Physical Chemistry and Electrochemistry, Leibniz Universität Hannover, Callinstr. 3A, 30167 Hannover, Germany

jannika.lauth@pci.uni-hannover.de

Authors

Fuzhao Li - Cluster of Excellence PhoenixD (Photonics, Optics, and Engineering – Innovation Across Disciplines), Hannover, Germany; Institute for Technical Chemistry, Technische Universität Braunschweig, Hagenring 30, 38106 Braunschweig, Germany

Lars F. Klepzig - Cluster of Excellence PhoenixD (Photonics, Optics, and Engineering – Innovation Across Disciplines), Hannover, Germany; Institute of Physical Chemistry and Electrochemistry, Leibniz Universität Hannover, Callinstraße 3A, 30167 Hannover, Germany

Nils Keppler - Cluster of Excellence PhoenixD (Photonics, Optics, and Engineering – Innovation Across Disciplines), Hannover, Germany; Institute of Inorganic Chemistry, Leibniz Universität Hannover, Callinstraße 9, 30167 Hannover, Germany

Peter Behrens - Cluster of Excellence PhoenixD (Photonics, Optics, and Engineering – Innovation Across Disciplines), Hannover, Germany; Institute of Inorganic Chemistry, Leibniz Universität Hannover, Callinstraße 9, 30167 Hannover, Germany; Laboratory of Nano and Quantum Engineering, Schneiderberg 39, 30167 Hannover, Germany

Nadja C. Bigall - Cluster of Excellence PhoenixD (Photonics, Optics, and Engineering – Innovation Across Disciplines), Hannover, Germany; Institute of Physical Chemistry and Electrochemistry, Leibniz Universität Hannover, Callinstraße 3A, 30167 Hannover, Germany; Laboratory of Nano and Quantum Engineering, Schneiderberg 39, 30167 Hannover, Germany

Henning Menzel - Cluster of Excellence PhoenixD (Photonics, Optics, and Engineering – Innovation Across Disciplines), Hannover, Germany; Institute for Technical Chemistry, Technische Universität Braunschweig, Hagenring 30, 38106 Braunschweig, Germany

Jannika Lauth - Cluster of Excellence PhoenixD (Photonics, Optics, and Engineering – Innovation Across Disciplines), Hannover, Germany; Institute of Physical Chemistry and Electrochemistry, Leibniz Universität Hannover, Callinstraße 3A, 30167 Hannover, Germany; Laboratory of Nano and Quantum Engineering, Schneiderberg 39, 30167 Hannover, Germany

Author Contributions

The manuscript was written with contributions of all authors. All authors have given approval to the final version of the manuscript. ‡Fuzhao Li and Lars F. Klepzig contributed equally to this work.

Notes

The authors declare no competing financial interest.

ACKNOWLEDGMENTS

We are grateful to Li Zhao and Hans-Hermann Johannes (IHF TU Braunschweig) for the profilometry measurements and to Stephanie Michel (IPAT TU Braunschweig) for the characterization of the nanocomposites by AFM. The authors thank the Laboratory of Nano and Quantum Engineering (LNQE) in Hannover for access to the TEM.

The project leading to these results was funded by the Deutsche Forschungsgemeinschaft (DFG, German Research Foundation) under Germany's Excellence Strategy within the Cluster of Excellence PhoenixD (EXC 2122, Project ID 390833453). J.L. gratefully acknowledges funding by the Caroline Herschel program of the Leibniz Universität Hannover.

ABBREVIATIONS

2D, two-dimensional; AAS, atomic absorption spectroscopy; AFM, atomic force microscopy; DLS, dynamic light scattering; FWHM, full width at half maximum; LbL, layer-by-layer; ML, monolayer; MUA, 11-mercapto-undecanoic acid; NC, nanocrystals; NPL, nanoplatelet; OD, optical density; ODE, 1-octadecene; PAAm, poly(allylamine); PDDA, poly(diallyldimethylammonium chloride); PEI, poly(ethylenimine); PEL, polyelectrolyte; PL, photoluminescence; LT, lifetime; PLQY, photoluminescence quantum yield; PSS, poly(styrenesulfonic acid); RET, resonance energy transfer; SEM, scanning electron microscopy; TEM, transmission electron microscopy; TCSPC, time-correlated single photon counting.

References

(1) Shendre, S., Delikanli, S., Li, M., Dede, D., Pan, Z., Ha, S. T., Fu, Y. H., Hernández-Martínez, P. L., Yu, J., Erdem, O., Kuznetsov, A. I., Dang, C., Sum, T. C., Demir, H. V. Ultrahigh-efficiency aqueous flat nanocrystals of CdSe/CdS@Cd1-xZnxS colloidal core/crown@alloyed-shell quantum wells. *Nanoscale* **2018**, *11*, 301–310.

(2) Tessier, M. D., Spinicelli, P., Dupont, D., Patriarche, G., Ithurria, S., Dubertret, B. Efficient Exciton Concentrators Built from Colloidal Core/Crown CdSe/CdS Semiconductor Nanoplatelets. *Nano Lett*. **2014**, *14*, 207-213.

(3) Tenney, S. M., Vilchez, V., Sonnleitner, M. L., Huang, C., Friedman, H. C., Shin, A. J., Atallah, T. L., Deshmukh, A. P., Ithurria, S., Caram, J. R. Mercury Chalcogenide Nanoplatelet-Quantum Dot Heterostructures as a New Class of Continuously Tunable Bright Shortwave Infrared Emitters. *J. Phys. Chem. Lett*. **2020**, *11*, 3473–3480.

(4) Manteiga Vázquez, F., Yu, Q., Klepzig, L. F., Siebbeles, L. D. A., Crisp, R. W., Lauth, J. Probing Excitons in Ultrathin PbS Nanoplatelets with Enhanced Near-Infrared Emission. *J. Phys. Chem. Lett*. **2021**, *12*, 680–685.

(5) Schlosser, A., Graf, R. T., Bigall, N. C. CdS crown growth on CdSe nanoplatelets: core shape matters. *Nanoscale Adv*. **2020**, *2*, 4604–4614.

(6) Guzelturk, B., Kelestemur, Y., Olutas, M., Delikanli, S., Demir, H. V. Amplified spontaneous emission and lasing in colloidal nanoplatelets. *ACS Nano* **2014**, *8*, 6599–6605.

(7) Chen, Z., Nadal, B., Mahler, B., Aubin, H., Dubertret, B. Quasi-2D Colloidal Semiconductor Nanoplatelets for Narrow Electroluminescence. *Adv. Funct. Mater*. **2014**, *24*, 295–302.

(8) Yang, Y., Zhang, C., Qu, X., Zhang, W., Marus, M., Xu, B., Wang, K., Sun, X. W. High Quantum Yield Colloidal Semiconducting Nanoplatelets and High Color Purity Nanoplatelet QLED. *IEEE Trans. Nanotechnol.* **2019**, *18*, 220–225.

(9) Kelestemur, Y., Olutas, M., Delikanli, S., Guzelturk, B., Akgul, M. Z., Demir, H. V. Type-II colloidal quantum wells: CdSe/CdTe core/crown heteronanoplatelets. *J. Phys. Chem. C* **2015**, *119*, 2177-2185.

(10) Hung, H.-I., Klein, O. J., Peterson, S. W., Rokosh, S. R., Osseiran, S., Nowell, N. H., Evans, C. L. PLGA nanoparticle encapsulation reduces toxicity while retaining the therapeutic efficacy of EtNBS-PDT in vitro. *Sci. Rep.* **2016**, *6*, 33234.

(11) Shiman, D. I., Sayevich, V., Meerbach, C., Nikishau, P. A., Vasilenko, I. V., Gaponik, N., Kostjuk, S. V., Lesnyak, V. Robust Polymer Matrix Based on Isobutylene (Co)polymers for Efficient Encapsulation of Colloidal Semiconductor Nanocrystals. *ACS Appl. Nano Mater.* **2019**, *2*, 956–963.

(12) Guzelturk, B., Menk, F., Philipps, K., Kelestemur, Y., Olutas, M., Zentel, R., Demir, H. V. Colloidal Nanoplatelet/Conducting Polymer Hybrids: Excitonic and Material Properties. *J. Phys. Chem. C* **2016**, *120*, 3573–3582.

(13) Lesser, C., Gao, M., Kirstein, S. Highly luminescent thin films from alternating deposition of CdTe nanoparticles and polycations. *Mater. Sci. Eng. C Mater. Biol. Appl.* **1999**, *8-9*, 159–162.

(14) Decher, G. Fuzzy Nanoassemblies: Toward Layered Polymeric Multicomposites. *Science* **1997**, *277*, 1232–1237.

(15) Shimazaki, Y., Mitsuishi, M., Ito, S., Yamamoto, M. Preparation of the Layer-by-Layer Deposited Ultrathin Film Based on the Charge-Transfer Interaction. *Langmuir* **1997**, *13*, 1385–1387.

(16) Podsiadlo, P., Tang, Z., Shim, B. S., Kotov, N. A. Counterintuitive effect of molecular strength and role of molecular rigidity on mechanical properties of layer-by-layer assembled nanocomposites. *Nano Lett*. **2007**, *7*, 1224–1231.

(17) Borges, J., Mano, J. F. Molecular interactions driving the layer-by-layer assembly of multilayers. *Chem*. *Rev*. **2014**, *114*, 8883–8942.

(18) Decher G., Schlenoff J. B., Eds. *Multilayer thin films: Sequential assembly of nanocomposite materials*; Wiley-VCH: Weinheim, 2003.

(19) Waraich, S. M., Hering, B., Burghard, Z., Bill, J., Behrens, P., Menzel, H. Fabrication and characterization of biocompatible nacre-like structures from α -zirconium hydrogen phosphate hydrate and chitosan. *J*. *Colloid Interface Sci*. **2012**, *367*, 74–82.

(20) Gao, M., Lesser, C., Kirstein, S., Möhwald, H., Rogach, A. L., Weller, H. Electroluminescence of different colors from polycation/CdTe nanocrystal self-assembled films. *Int*. *J*. *Appl*. *Phys*. **2000**, *87*, 2297–2302.

(21) Tang, Z., Wang, Y., Kotov, N. A. Semiconductor Nanoparticles on Solid Substrates: Film Structure, Intermolecular Interactions, and Polyelectrolyte Effects. *Langmuir* **2002**, *18*, 7035–7040.

(22) Almodóvar, J., Place, L. W., Gogolski, J., Erickson, K., Kipper, M. J. Layer-by-layer assembly of polysaccharide-based polyelectrolyte multilayers: a spectroscopic study of hydrophilicity, composition, and ion pairing. *Biomacromolecules* **2011**, *12*, 2755–2765.

(23) Boudou, T., Crouzier, T., Ren, K., Blin, G., Picart, C. Multiple functionalities of polyelectrolyte multilayer films: new biomedical applications. *Adv. Mater.* **2010**, *22*, 441–467.

(24) He, L., Dexter, A. F., Middelberg, A. P. Biomolecular engineering at interfaces. *Chem. Eng. Sci.* **2006**, *61*, 989–1003.

(25) Lin, Y.-W., Tseng, W.-L., Chang, H.-T. Using a Layer-by-Layer Assembly Technique to Fabricate Multicolored-Light-Emitting Films of CdSe@CdS and CdTe Quantum Dots. *Adv. Mater.* **2006**, *18*, 1381–1386.

(26) Wang, Y., Tang, Z., Correa-Duarte, M. A., Liz-Marzán, L. M., Kotov, N. A. Multicolor luminescence patterning by photoactivation of semiconductor nanoparticle films. *J. Am. Chem. Soc.* **2003**, *125*, 2830–2831.

(27) Hao, E., Lian, T. Layer-by-Layer Assembly of CdSe Nanoparticles Based on Hydrogen Bonding. *Langmuir* **2000**, *16*, 7879–7881.

(28) Kelestemur, Y., Guzelturk, B., Erdem, O., Olutas, M., Gungor, K., Demir, H. V. Platelet-in-Box Colloidal Quantum Wells: CdSe/CdS@CdS Core/Crown@Shell Heteronanoplatelets. *Adv. Funct. Mater.* **2016**, *26*, 3570–3579.

(29) Pedetti, S., Ithurria, S., Heuclin, H., Patriarche, G., Dubertret, B. Type-II CdSe/CdTe Core/Crown Semiconductor Nanoplatelets. *J. Am. Chem. Soc.* **2014**, *136*, 16430-16438.

(30) Kodanek, T., Banbela, H. M., Naskar, S., Adel, P., Bigall, N. C., Dorfs, D. Phase transfer of 1- and 2-dimensional Cd-based nanocrystals. *Nanoscale* **2015**, *7*, 19300-19309.

(31) Scheepers, D., Chatillon, B., Borneman, Z., Nijmeijer, K. Influence of charge density and ionic strength on diallyldimethylammonium chloride (DADMAC)-based polyelectrolyte multilayer membrane formation. *J. Membr. Sci.* **2021**, *617*, 118619.

(32) Borkovec, M., Koper, G. J. M. Proton Binding Characteristics of Branched Polyelectrolytes. *Macromolecules* **1997**, *30*, 2151–2158.

(33) Zhang, H., He, H.-X., Wang, J., Mu, T., Liu, Z.-F. Force titration of amino group-terminated self-assembled monolayers using chemical force microscopy. *Appl. Phys. A Mater. Sci. Process.* **1998**, *66*, S269-S271.

(34) Vezenov, D. V., Noy, A., Rozsnyai, L. F., Lieber, C. M. Force Titrations and Ionization State Sensitive Imaging of Functional Groups in Aqueous Solutions by Chemical Force Microscopy. *J. Am. Chem. Soc.* **1997**, *119*, 2006–2015.

(35) Zaibudeen, A. W., Philip, J. Behavior of a strong polyelectrolyte, poly(diallyldimethylammonium chloride) physisorbed at oil-water interface under different environments A comparison with a weak polyelectrolyte. *Colloids Surf. A* **2018**, *550*, 209–221.

(36) Ithurria, S., Tessier, M. D., Mahler, B., Lobo, R. P. S. M., Dubertret, B., Efros, A. L. Colloidal nanoplatelets with two-dimensional electronic structure. *Nat. Mater.* **2011**, *10*, 936-941.

(37) Bouet, C., Tessier, M. D., Ithurria, S., Mahler, B., Nadal, B., Dubertret, B. Flat Colloidal Semiconductor Nanoplatelets. *Chem. Mater.* **2013**, *25*, 1262–1271.

(38) Sydow, S., Cassan, D. de, Hänsch, R., Gengenbach, T. R., Easton, C. D., Thissen, H., Menzel, H. Layer-by-layer deposition of chitosan nanoparticles as drug-release coatings for PCL nanofibers. *Biomater. Sci.* **2018**, *7*, 233–246.

(39) Lavalle, P., Picart, C., Mutterer, J., Gergely, C., Reiss, H., Voegel, J.-C., Senger, B., Schaaf, P. Modeling the Buildup of Polyelectrolyte Multilayer Films Having Exponential Growth. *J. Phys. Chem. B* **2004**, *108*, 635–648.

(40) Rogach, A. L., Koktysh, D. S., Harrison, M., Kotov, N. A. Layer-by-Layer Assembled Films of HgTe Nanocrystals with Strong Infrared Emission. *Chem. Mater.* **2000**, *12*, 1526–1528.

(41) Scott, R., Heckmann, J., Prudnikau, A. V., Antanovich, A., Mikhailov, A., Owschimikow, N., Artemyev, M., Climente, J. I., Woggon, U., Grosse, N. B., Achtstein, A. W. Directed emission of CdSe nanoplatelets originating from strongly anisotropic 2D electronic structure. *Nat. Nanotechnol.* **2017**, *12*, 1155–1160.

(42) Lin, W., Zou, W., Du, Z., Li, H., Zhang, C. Study on the optical properties of CdSe QDs with different ligands in specific matrix. *J. Nanopart. Res.* **2013**, *15*.

(43) Correa-Duarte, M. A., Giersig, M., Kotov, N. A., Liz-Marzán, L. M. Control of Packing Order of Self-Assembled Monolayers of Magnetite Nanoparticles with and without SiO 2 Coating by Microwave Irradiation. *Langmuir* **1998**, *14*, 6430–6435.

(44) Bucur, C. B., Sui, Z., Schlenoff, J. B. Ideal mixing in polyelectrolyte complexes and multilayers: entropy driven assembly. *J. Am. Chem. Soc.* **2006**, *128*, 13690–13691.

(45) Voigt, U., Jaeger, W., Findenegg, G. H., Klitzing, R. v. Charge Effects on the Formation of Multilayers Containing Strong Polyelectrolytes. *J. Phys. Chem. B* **2003**, *107*, 5273–5280.

(46) Manning, G. S. Limiting Laws and Counterion Condensation in Polyelectrolyte Solutions I. Colligative Properties. *J. Chem. Phys.* **1969**, *51*, 924–933.

(47) Muthukumar, M. Theory of counter-ion condensation on flexible polyelectrolytes: adsorption mechanism. *J. Chem. Phys.* **2004**, *120*, 9343–9350.

(48) Zan, X., Hoagland, D. A., Wang, T., Su, Z. Ion Dispositions in Polyelectrolyte Multilayer Films. *Macromolecules* **2012**, *45*, 8805–8812.

(49) Zhang, Z., Thung, Y. T., Chen, X., Wang, L., Fan, W., Ding, L., Sun, H. Study of Complex Optical Constants of Neat Cadmium Selenide Nanoplatelets Thin Films by Spectroscopic Ellipsometry. *J. Phys. Chem. Lett.* **2021**, *12*, 191–198.

(50) Mahler, B., Nadal, B., Bouet, C., Patriarche, G., Dubertret, B. Core/Shell Colloidal Semiconductor Nanoplatelets. *J. Am. Chem. Soc.* **2012**, *134*, 18591-18598.

(51) Naskar, S., Miethe, J. F., Sánchez-Paradinas, S., Schmidt, N., Kanthasamy, K., Behrens, P., Pfnür, H., Bigall, N. C. Photoluminescent Aerogels from Quantum Wells. *Chem. Mater.* **2016**, *28*, 2089-2099.

(52) Niculescu, E. C. Interlevel transitions in core–shell nanodots with dielectric environment. *Superlattices Microstruct.* **2012**, *51*, 814–824.

(53) Yang, Y., Zheng, Y., Cao, W., Titov, A., Hyvonen, J., Manders, J. R., Xue, J., Holloway, P. H., Qian, L. High-efficiency light-emitting devices based on quantum dots with tailored nanostructures. *Nat. Photonics* **2015**, *9*, 259–266.

(54) Nasilowski, M., Spinicelli, P., Patriarche, G., Dubertret, B. Gradient CdSe/CdS Quantum Dots with Room Temperature Biexciton Unity Quantum Yield. *Nano Lett.* **2015**, *15*, 3953–3958.

(55) Taylor, D. A., Teku, J. A., Cho, S., Chae, W.-S., Jeong, S.-J., Lee, J.-S. Importance of Surface Functionalization and Purification for Narrow FWHM and Bright Green-Emitting InP Core–Multishell Quantum Dots via a Two-Step Growth Process. *Chem. Mater.* **2021**, *33*, 4399–4407.

(56) Zlateva, G., Zhelev, Z., Bakalova, R., Kanno, I. Precise size control and synchronized synthesis of six colors of CdSe quantum dots in a slow-increasing temperature gradient. *Inorg. Chem.* **2007**, *46*, 6212–6214.

(57) Saidzhonov, B. M., Zaytsev, V. B., Vasiliev, R. B. Effect of PMMA polymer matrix on optical properties of CdSe nanoplatelets. *J. Lumin.* **2021**, *237*, 118175.

(58) Wuister, S. F., Mello Donegá, C. de, Meijerink, A. Influence of Thiol Capping on the Exciton Luminescence and Decay Kinetics of CdTe and CdSe Quantum Dots. *J. Phys. Chem. B* **2004**, *108*, 17393–17397.

(59) Rogach, A. L., Franzl, T., Klar, T. a., Feldmann, J., Gaponik, N., Lesnyak, V., Shavel, A., Eychmüller, A., Rakovich, Y. P., Donegan, J. F. Aqueous Synthesis of Thiol-Capped CdTe Nanocrystals: State-of-the-Art. *J. Phys. Chem. C* **2007**, *111*, 14628–14637.

(60) Davis, N. J. L. K., Allardice, J. R., Xiao, J., Karani, A., Jellicoe, T. C., Rao, A., Greenham, N. C. Improving the photoluminescence quantum yields of quantum dot films through a donor/acceptor system for near-IR LEDs. *Mater. Horiz.* **2019**, *6*, 137–143.

(61) Yang, P., Li, C. L., Murase, N. Highly photoluminescent multilayer QD-glass films prepared by LbL self-assembly. *Langmuir* **2005**, *21*, 8913–8917.

(62) Shavel, A., Gaponik, N., Eychmüller, A. The Assembling of Semiconductor Nanocrystals. *Eur. J. Inorg. Chem.* **2005**, *2005*, 3613–3623.

(63) Würth, C., Grabolle, M., Pauli, J., Spieles, M., Resch-Genger, U. Relative and absolute determination of fluorescence quantum yields of transparent samples. *Nat. Protoc.* **2013**, *8*, 1535–1550.

Supporting Information

Layer-by-Layer Deposition of 2D CdSe/CdS Nanoplatelets and Polymers for Photoluminescent Composite Materials

Fuzhao Li[†], Lars F. Klepzig[†], Nils Keppler, Peter Behrens, Nadja C. Bigall, Henning Menzel[*], Jannika Lauth[*]

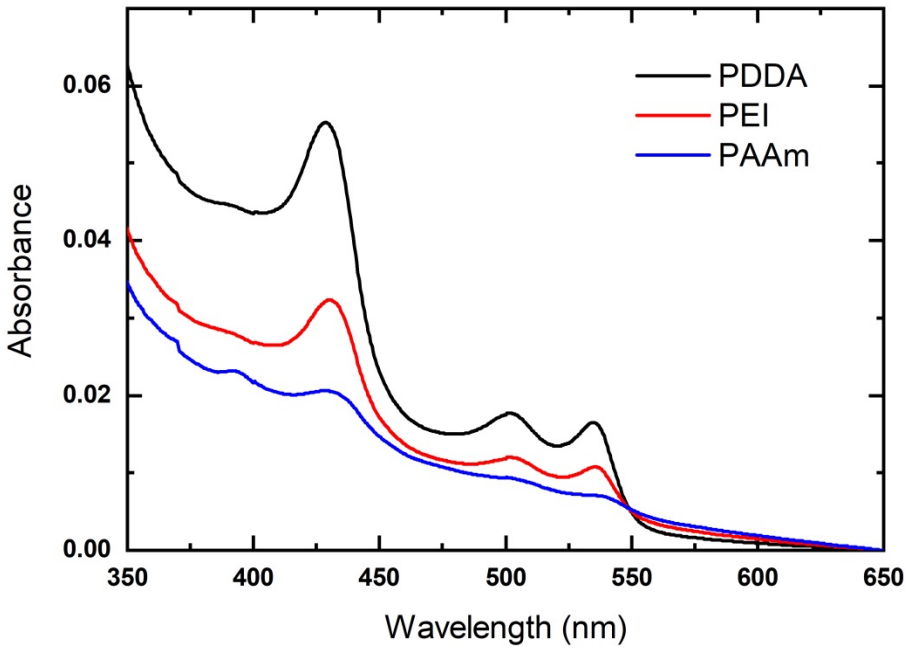

Figure S1: Absorbance and PL of three bilayer LbL coatings using PDDA (black), PEI (red) and PAAm (blue) as PELs with a NPL solution at pH 6. LbL layers deposited with PAAm exhibit excitonic feature loss and strongly decreased PL due to unfavorable interaction between the NPLs and the primary amine of the PAH.

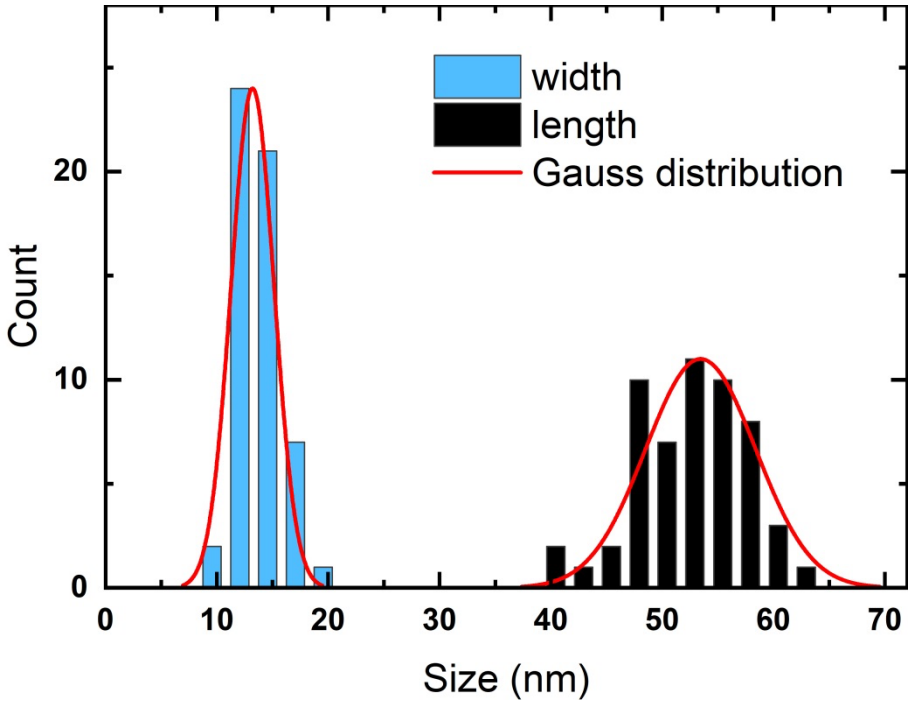

Figure S2: Size histogram of CdSe/CdS NPLs synthesized with a mean width of 13.2 ± 1.9 nm and a mean length of 53.5 ± 4.9 nm. The sizes are averaged over 60 NPLs counted from TEM images prepared from hexane solution.

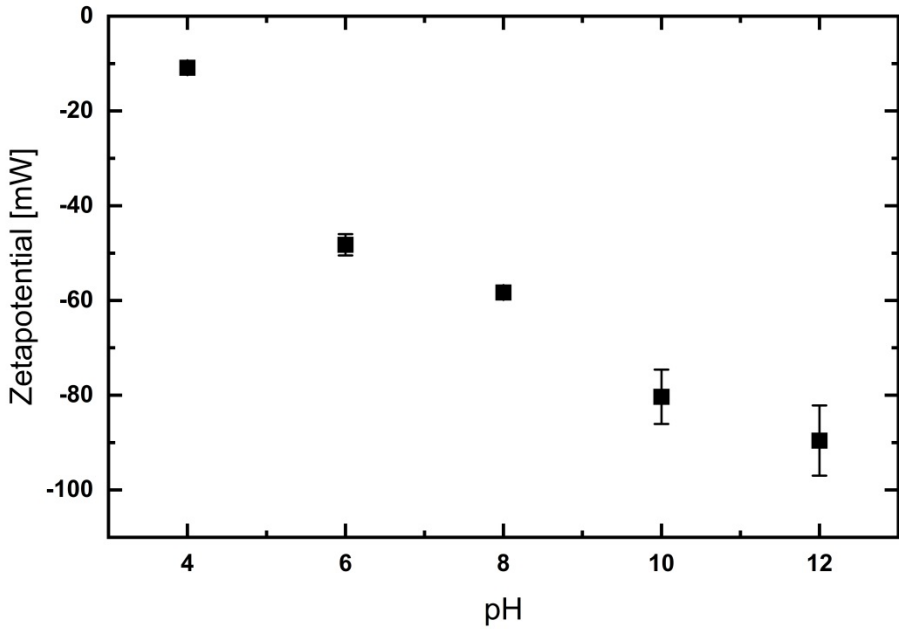

Figure S3: pH-dependent zeta potential of MUA-capped CdSe/CdS NPLs exhibiting zeta potential values ≤ -50 mV for pH ≥ 6, indicating a stable dispersion.

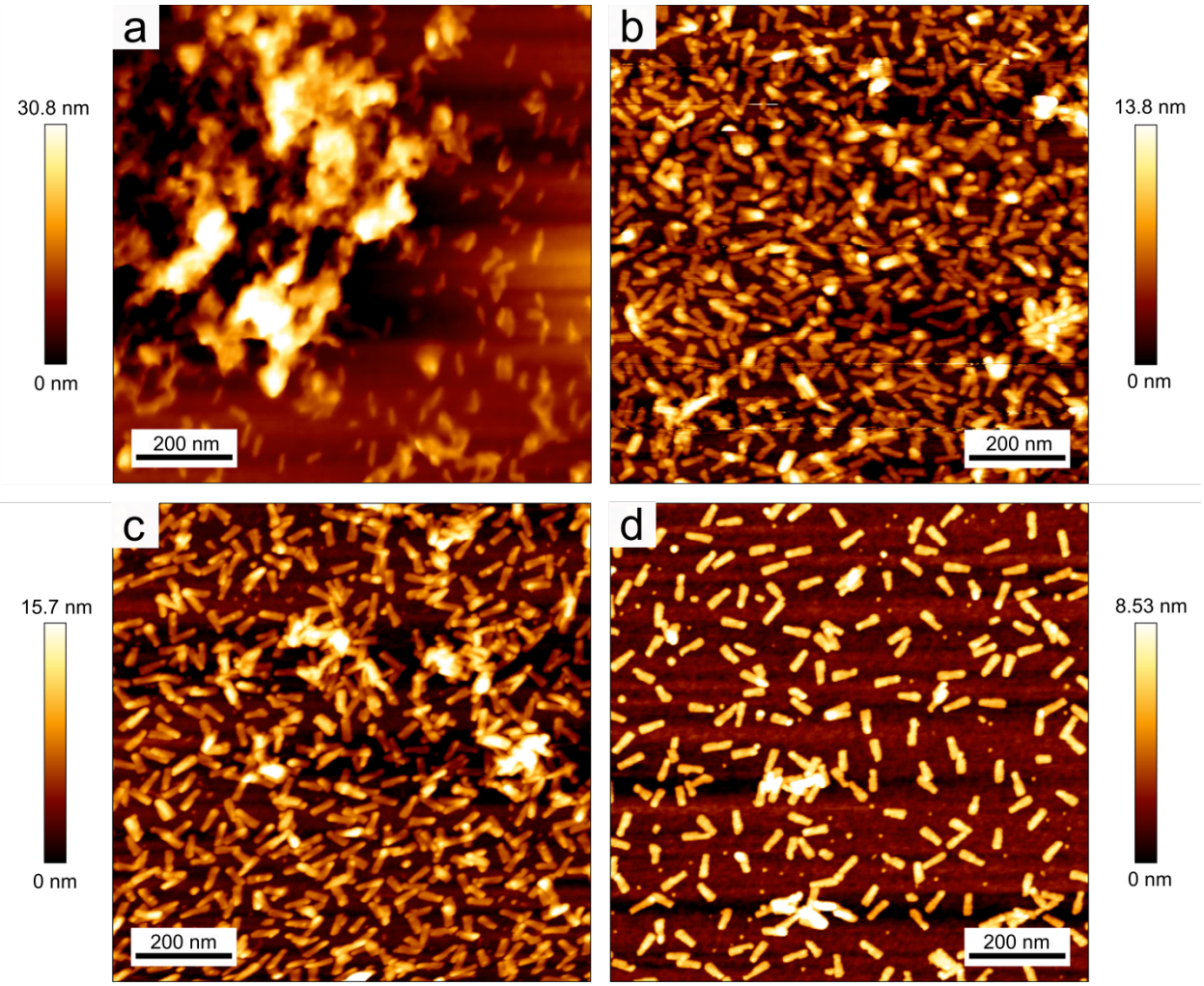

Figure S4: 1 x 1 μm^2 AFM height images of one NPL/PEL bilayer on silicon substrates using a) PEI with NPLs at pH 6, b) PEI with NPLs at pH of 10, c) PDDA with NPLs at pH 6, and d) PDDA with NPLs at pH 10, corresponding to the AFM phase images shown in Figure 3.

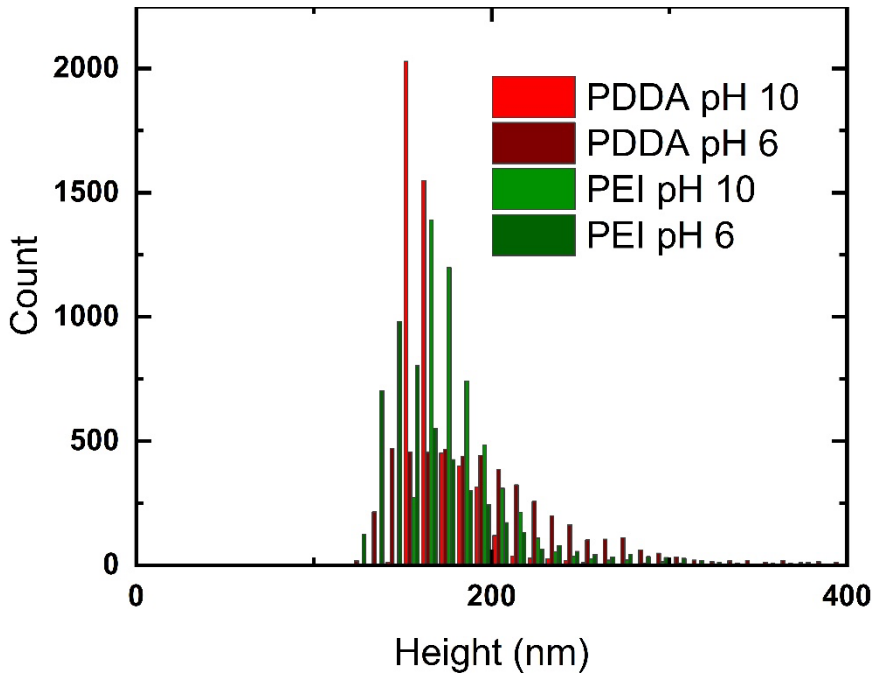

Figure S5: Histogram of the height of nanocomposite films consisting of 50 PEL/NPL bilayers on Si as determined by profilometry. While films obtained with CdSe/CdS NPL dispersions held at pH 6 show larger deviations, dispersions at pH 10 lead to narrow height distributions as discussed in the main text and shown by the surface roughness.

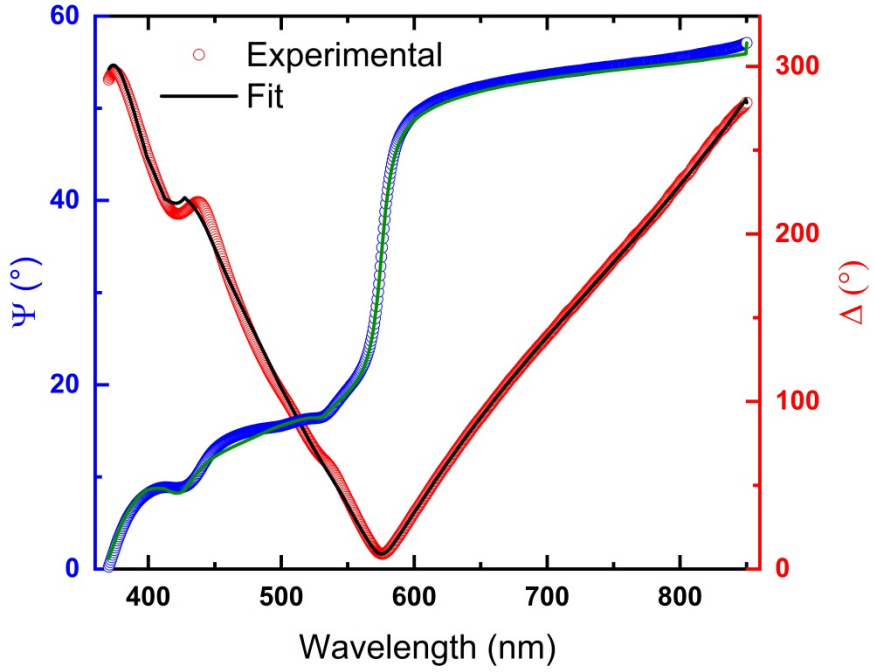

Figure S6: Exemplary comparison of the raw data and the fit of the ellipsometry measurement of a 50 bilayer LbL coating with PDDA as PEL and pH 10 for the NPL dispersion. The fit exhibits a MSE of 2.55.

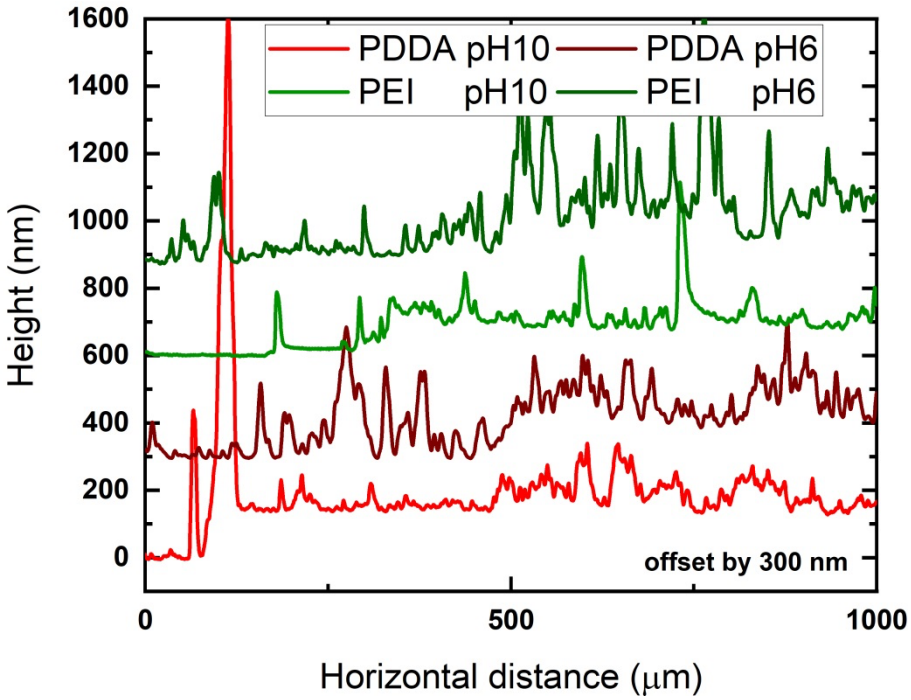

Figure S7: Exemplary profilometry measurements of the height of LbL coatings with 50 PEL/NPL bilayers on Si. The difference between the blank substrate (left) and the coating (right) is shown, as well as the differences in surface roughness as is discussed in the main text. The graphs are shown with a vertical offset of 300 nm for clarity.

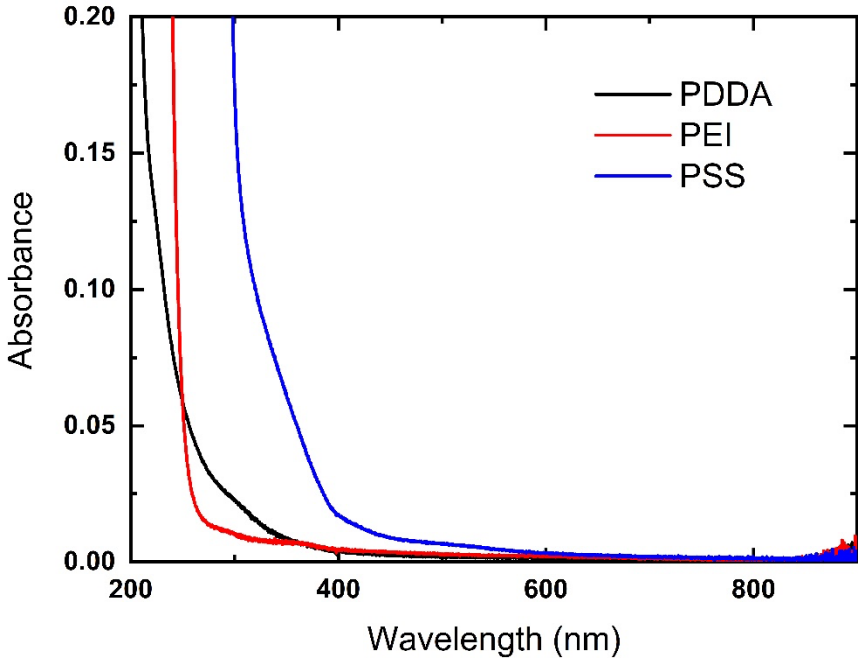

Figure S8: Absorbance of the polymers (1 mg ml^{-1} in H_2O) used for PEL/NPL nanocomposite coatings. PDDA and PEI do not show absorbance close to the NPL absorbance range (≤ 550 nm). PSS exhibits rather low absorbance close to the NPL absorbance range. We conclude that the absorbance features of the nanocomposites are dominated by the optical properties of the CdSe/CdS NPLs as is discussed in the main manuscript.

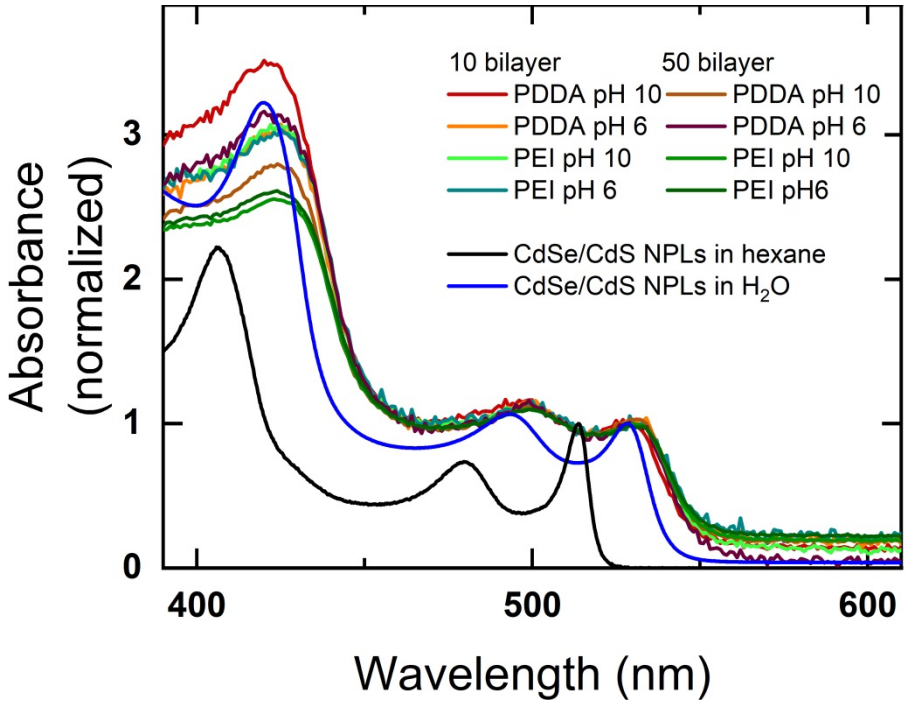

Figure S9: Absorbance of the PEL/NPL nanocomposites prepared under different conditions and normalized to the first excitonic absorption peak of the NPLs. The optical properties of the nanocomposites are dominated by the CdSe/CdS NPLs, which stay unaffected by the choice of polymer, the pH value of the NPL dispersion, and the number of bilayers.

Photoluminescence quantum yield (PLQY) measurements

Steady-state PL spectra were acquired using an Edinburgh FLS 1000 UV-Vis-NIR photoluminescence spectrometer. The optical characterization of NPL dispersions was carried out using quartz cuvettes with a path length of 10 mm. Layer-by-layer coatings on glass were measured using a solid state sample holder. The steady-state PL was collected by exciting the samples at 450 nm (optical density < 0.2 at the excitation wavelength) with a xenon lamp and utilizing a PMT detector. The PLQY was determined inside an integrating sphere, measuring the scattering and the emission in the of both, a blank and the sample. Equation (1) was used for the determination of the PLQY[S1]:

$$PLQY = \frac{E_B - E_A}{S_A - S_B} \qquad (1)$$

With E the emission area (area under the curve), S the area of the scattering, i.e. the non-absorbed light at the excitation wavelength, k the ratio of the detector sensitivities, and the indices A and B marking the reference and the sample, respectively.

S1: Würth, C.; Geissler, D.; Behnke, T.; Kaiser, M.; Resch-Genger, U. Critical Review of The Determination of Photoluminescence Quantum Yields of Luminescent Reporters. *Anal. Bioanal. Chem.* **2015**, *407*, 59–78.